Soft Matter

PAPER

View Article Online
View Journal | View Issue

Published on 11 December 2018. Downloaded by Gothenburg University Library on 1/21/2019 5:18:15 AM.

Check for updates

Cite this: *Soft Matter*, 2019, 15, 442

Infinite coordination polymer networks: metallogelation of aminopyridine conjugates and *in situ* silver nanoparticle formation†

Rajendhraprasad Tatikonda, [a] Evgeny Bulatov, [a] Zülal Özdemir, [bc] Nonappa [*de] and Matti Haukka [*a]

Received 2nd October 2018,
Accepted 10th December 2018

DOI: 10.1039/c8sm02006j

rsc.li/soft-matter-journal

Herein we report silver(I) directed infinite coordination polymer network (ICPN) induced self-assembly of low molecular weight organic ligands leading to metallogelation. Structurally simple ligands are derived from 3-aminopyridine and 4-aminopyridine conjugates which are composed of either pyridine or 2,2′-bipyridine cores. The cation specific gelation was found to be independent of the counter anion, leading to highly entangled fibrillar networks facilitating the immobilization of solvent molecules. Rheological studies revealed that the elastic storage modulus (G') of a given gelator molecule is counter anion dependent. The metallogels derived from ligands containing a bipyridine core displayed higher G' values than those with a pyridine core. Furthermore, using single crystal X-ray diffraction studies and $^{1}H-^{15}N$ two-dimensional (2D) correlation NMR spectroscopy, we show that the tetracoordination of silver ions enables simultaneous coordination polymerization and metallosupramolecular cross-linking. The resulting metallogels show spontaneous, *in situ* nanoparticle (d < 2–3 nm) formation without any additional reducing agents. The silver nanoparticle formation was followed using spectroscopic studies, and the self-assembled fibrillar networks were imaged using transmission electron microscopy (TEM) imaging.

Introduction

Metal–ligand (M–L) interaction induced assembly of small organic molecules (*i.e.* metallosupramolecular chemistry) has evolved as one of the versatile ways to build topologically diverse metallosupramolecular structures.[1] The ability to tune the interaction strength and number of metal binding sites with synthetically simple organic ligands offers rapid access to one, two, or three-dimensional metallosupramolecular polymeric structures.[2] In certain cases, the resulting superstructures undergo hierarchical assembly to highly entangled fibrillar networks and immobilize the solvents leading to gelation. The resulting gels are known as metallosupramolecular gels or simply metallogels.[3] Metallogels are either produced from discrete coordination compounds,[4] infinite coordination polymers (ICPs),[5] or cross-linked CPs.[6] In discrete metal complexes, the supramolecular interactions between the gelator molecules promote the self-assembly, whereas the metal–ligand coordination often acts as a secondary force in gelation. Gels derived from discrete complexes display reversible gel–sol transition upon subjecting them to external stimuli (*e.g.*, temperature, light, pH *etc.*). On the other hand, in coordination polymers (CPs), the primary driving force is metal–ligand coordination, leading to infinite coordination polymeric networks (ICPNs) and the coordination polymers act as gelators. The gels derived from ICPs often show resistance to reversible gel–sol transition.[7] The presence of metal ions provides some of the unique responsiveness to temperature,[8] mechanical perturbance,[9] light,[10] oxidation–reduction,[11] electric- and magnetic fields.[12] The structure and coordination ability of an organic ligand has an impact on topologies and functional properties of metal complexes. Therefore, selection of the organic ligand is vital in preparing functional metallogels, where the crystal engineering approach has played an

[a] *Department of Chemistry, University of Jyväskylä, P. O. Box 35, FI-40014 Jyväskylä, Finland. E-mail: matti.o.haukka@jyu.fi*
[b] *Department of Chemistry of Natural Compounds, Faculty of Food and Biochemical Technology, University of Chemistry and Technology, Technicka 5, 16628 Prague 6, Czech Republic*
[c] *Institute of Experimental Botany AS CR, Isotope Laboratory, Videnska 1083, 14220 Prague 4, Czech Republic*
[d] *Department of Applied Physics, Aalto University School of Science, Puumiehenkuja 2, FI-02150 Espoo, Finland. E-mail: nonappa@aalto.fi*
[e] *Department of Bioproducts and Biosystems, Aalto University School of Chemical Engineering, Kemistintie 1, FI-02150 Espoo, Finland*

† Electronic supplementary information (ESI) available: Synthesis of ligands, 1D and 2D NMR spectra of ligands and their silver complexes, single crystal X-ray data, additional TEM micrographs and rheological and photoluminescence studies. CCDC 1823427–1823433. For ESI and crystallographic data in CIF or other electronic format see DOI: 10.1039/c8sm02006j

This journal is © The Royal Society of Chemistry 2019

Published on 11 December 2018. Downloaded by Gothenburg University Library on 1/21/2019 5:18:15 AM.

important role. Ligands containing different metal binding sites have been studied in metallogelation, for example, polypyridyl compounds, porphyrin derivatives, amines, thiols, azoles, dendrimers, and carboxylates.[13–17] To obtain a metallogel, the ligand should able to participate in one or more than one noncovalent intermolecular interaction (such as H-bonding, π-stacking, van der Waals interaction, electrostatic interactions) in addition to metal coordination.[18] Various approaches have been reported in the literature on the preparation of metallogels, including subcomponent self-assembly.[19] Potential applications of metallogels in cosmetics, lubrication, magnetic materials and sensors for dye molecules have been demonstrated in the literature.[20–22] Furthermore, properties such as self-assembly induced luminescence provide promising applications in optoelectronics[23] and in developing vapochromic sensors.[24] Recently, terpyridine ligands containing perfluoroalkyl chains have been reported to exhibit anion selective gelation and rapid self-healing properties.[25] The transition metal containing gels such as palladium have also been shown to improve the catalytic activities.[26]

Metallogels containing Ag(I) as metal ions and pyridine derivatives as ligands, represent one of the extensively studied systems. This is attributed to their antimicrobial and photophysical properties.[27] In addition to its role as a coordinating agent, Ag(I) also serves as a precursor for *in situ* silver nanoparticle (AgNP) formation without any additional stabilizing agents.[28] *In situ* silver nanoparticle (AgNP) formation in metallogels involving pyridine and bipyridyl molecules have been reported either under ambient conditions, UV irradiation or sodium borohydride reduction.[29,30] However, in a majority of the reports, the resulting AgNPs were relatively large (>5 nm). We have recently reported synthetically simple bipyridyl based gelators displaying a remarkable difference in their ability for size and shape selective AgNP formation depending on the source of reducing agent and gelator chemical structure.[31] Furthermore, the binding of Ag(I) to form polymeric structures *via* tetracoordination of Ag(I) has been proposed based on 2D NMR spectroscopic studies. Understanding the specific metal–ligand interaction in hierarchical structure formation is important not only to gain insights into the gelation mechanism but also in the rational design of materials with desired morphology and mechanical properties.

ICPs have been studied mostly in the context of crystal engineering. Furthermore, it has been shown that structurally complex ligands prepared using a sophisticated ligand design allow tailorable colloidal microparticle formation with spherical morphologies.[32] Beyond crystal engineering and structure formation, there is a need to design strategically simple ligands for ICPN formation to provide access to novel multifunctional hybrid materials.

In this work, we report the synthesis, infinite coordination polymerization directed gelation, and self-assembly induced luminescence of aminopyridine conjugates (**1–4**, Fig. 1) in aqueous dimethyl sulfoxide as well as *in situ* silver nanoparticle ($d \leq 3$ nm) formation. Using single crystal X-ray diffraction studies, we show that tetracoordinated silver is responsible for metallosupramolecular polymerization in the solid state. Furthermore, the metal complexes in solution were studied using ^{1}H–^{15}N 2D NMR spectroscopy. Importantly, silver(I) directs coordination polymerization (CP) and supramolecular cross-linking between the polymeric chains thereby leading to highly entangled fibrillar network formation and also acts as a source for ultrasmall AgNPs. The gelation is cation specific, and their stability depends on the counter anion.

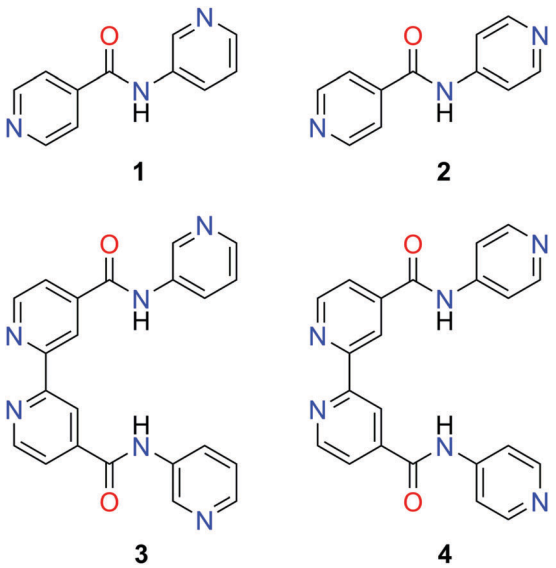

Fig. 1 Chemical structure of the ligands used in this study.

Results and discussion

The pyridyl amide ligands (**1** and **2**) were synthesized according to the reported literature procedure.[33] The synthesis of the bipyridyl amide ligands (**3** and **4**) was achieved by the reaction of 4,4′-dicarboxy-2,2′-bipyridine with 3-, or 4-aminopyridines in the presence of *N*-ethyl-*N*′-(3-dimethylaminopropyl carbodiimide) (EDC) in *N*,*N*-dimethyl formamide (DMF) solvent (see the ESI,† Scheme S1 and Fig. S1–S10 for NMR spectral data).

First, we discuss the structural properties of ligands **1–4** (Fig. 1). The solid-state structural details of ligands **1–2** have already been documented in the literature.[34] Therefore, no attempts were made to obtain their single crystals. Instead, efforts were made to grow single crystals and determine X-ray structures of ligands **3** and **4**. However, only ligand **4** resulted in quality single crystals either from acetonitrile, dimethyl sulfoxide (DMSO) or *N*,*N*-dimethylformamide (DMF) (Fig. 2).[35]

Ligand **3** either remained in solution or resulted in a precipitate. The solid-state structure of **4** obtained from acetonitrile (Fig. 2c) shows well organized intermolecular H-bonding (N–H···O = 2.18 Å) between the adjacent molecules through amide groups. The crystal packing also reveals the presence of weak intermolecular aromatic C═C–H···N and C═C–H···O H-bonding interactions. In addition to these weak H-bonds, the packing commences through off-set π···π interactions (3.3 Å). When ligand **4** was crystallized from DMSO (Fig. 2a) or DMF (Fig. 2b),

Published on 11 December 2018. Downloaded by Gothenburg University Library on 1/21/2019 5:18:15 AM.

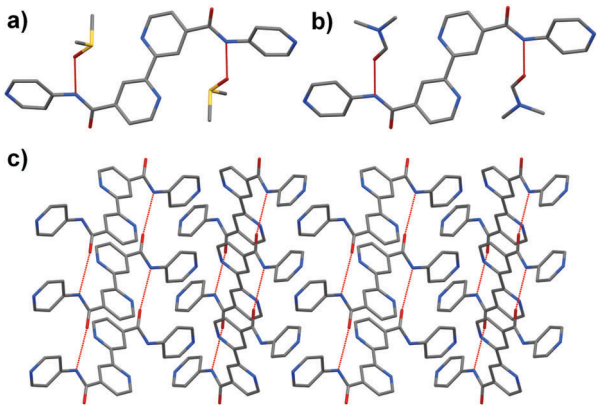

Fig. 2 X-ray single crystal structure: a molecular unit of **4** recrystallized from DMSO (a) and DMF (b) and crystal packing of well-organized H-bonding in **4** recrystallized from acetonitrile (c). Hydrogen atoms are omitted for clarity.

solvates were obtained, and the ligand molecule participated in H-bonding with the oxygen atom of solvent molecules.

Ligands **1** and **2** have been previously studied for their hydrogelation ability without the addition of metal ions by Das *et al.*, and their experimental results have shown that only **2** was able to form a hydrogel.[34] Importantly, the previous study was carried out only in water and not using any solvent mixtures. In this study, ligands **1–4** were screened for gelation and metallogelation in various solvents. Firstly, ligands **1** and **2** were tested for gelation in methanol, ethanol, acetonitrile, tetrahydrofuran, *N*,*N*′-dimethylformamide (DMF), dimethyl sulfoxide (DMSO) and their mixtures with water. In all the tested solvents, ligands **1** and **2** either remained in solution or precipitated. However, when a mixture of DMSO : H_2O or DMF : H_2O was kept at 2 : 8 or 3 : 7 (v/v), ligand **1** remained in solution and **2** resulted in crystals (Fig. S11a, ESI†). Ligands **3** and **4**, on the other hand, were insoluble in the tested solvents except in DMSO and DMF. Furthermore, when a mixture of DMSO : H_2O or DMF : H_2O was used, ligands **3** and **4** resulted in precipitates (Fig. S11a, ESI†). The presence of tertiary nitrogen offers metal binding sites in all four ligands. Therefore, it was expected that the metal complexation affects the assembly of the ligands. To test this hypothesis various water soluble metal salts were tested as the metal source. Among all the tested metal ions, complexation with silver(I) ions lead to metallogels in aqueous DMSO or aqueous DMF indicating the cation specific metallogelation properties of the ligands. Therefore, systematic studies using six different silver salts *viz.* nitrate (NO_3^-), trifluoromethane sulfonate aka triflate (OTf^-), perchlorate (ClO_4^-), acetate (OAc^-), tetrafluoroborate (BF_4^-) and hexafluorophosphate (PF_6^-) were performed. Table 1 and Fig. 3 show the details of gelation studies of ligands **1–4** when mixed with different silver salts and corresponding photographs in a given ratio of DMSO : H_2O system, respectively.

The metallogelation was studied for bidentate ligand **1** in 2 : 8, 3 : 7 and 4 : 6 DMSO : H_2O (v/v) ratio. However, stable metallogels were obtained with 3 : 7 DMSO : H_2O solution. It should be noted that the solvent mixture has a considerable impact on metallogelation and no gelation was observed in

Table 1 Gelation studies of ligands **1–4** with various silver salts in a mixture of water and DMSO. (Note: G = gel, G* = gels are unstable and collapsed upon standing at room temperature for an hour, P = precipitate). Ag : L represents the metal to ligand molar ratio (Ag = silver, **L** = ligand)

DMSO : H_2O	**L**	Ag : L	NO_3^-	ClO_4^-	OTf^-	PF_6^-	BF_4^-	OAc^-
3 : 7	**1**	1 : 2	G	G*	G*	G	G	G
3 : 7	**2**	1 : 2	P	P	G	G	P	G
7 : 3	**3**	1 : 1	G	G	G	G	G	G
7 : 3	**4**	1 : 1	G*	G*	G*	G	G*	G

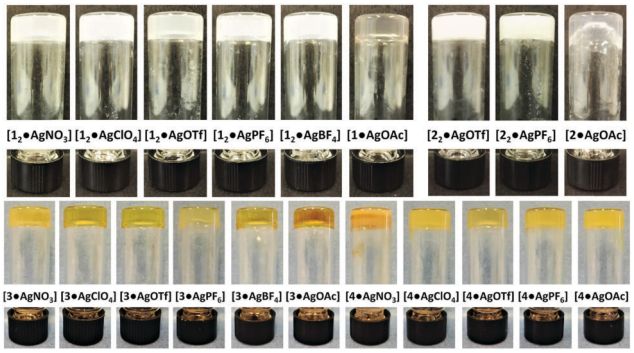

Fig. 3 Photographs of gels prepared from ligands **1–4** with various silver salts in aqueous DMSO.

pure DMSO or when the volume of DMSO exceeded the volume of water in the solution. Similar results were obtained also for ligand **2**. In order to find the optimum ligand-to-metal molar ratio, gelation studies were carried out using silver nitrate at 4 : 1, 2 : 1 and 1 : 1 ligand-to-metal (L : M) ratio.

The above study revealed that all the compositions resulted in gels. However, at an L : M ratio of 4 : 1 only a weak gel was formed. Gels obtained with a 1 : 1 ligand-to-silver ratio were found to be unstable and collapsed at room temperature within *ca.* 10 minutes (Fig. S11b, ESI†). However, stable gels were obtained when the L : M ratio was maintained at 2 : 1 indicating possible tetracoordination of silver ions. The ligand **2** was found to behave similarly. Therefore, further studies were performed using the 1 : 2 metal-to-ligand ratio and 3 : 7 DMSO : H_2O solvent ratio for ligands **1** and **2** (Fig. 3). The minimum gelation concentration (mgc) was found to be 0.8 wt% for both the tested ligands in 3 : 7 DMSO : H_2O. The gelation experiments of **1** resulted in metallogels with all the tested silver salts. However, gels obtained from **1** and Ag with ClO_4^- and OTf^- counter anions were found to be unstable and collapsed to precipitate. Unlike ligand **1**, ligand **2** gave metallogels only with the larger counter anions (OTf^-, PF_6^- and OAc^-) and resulted in precipitates with other silver salts (Fig. 3). The metallogelation of **1** and **2** was also observed in a mixture of DMF : H_2O (Fig. S11c, ESI†). However, during a gelation experiment, the addition of metal salts resulted in precipitates as the initial product. To obtain stable gels, the precipitate had to be redissolved by heating. The heating resulted in an immediate dark brown coloured unstable gel. The colour change is attributed to the rapid reduction of silver ions by DMF, which is well documented in the literature.[28d]

This journal is © The Royal Society of Chemistry 2019

Published on 11 December 2018. Downloaded by Gothenburg University Library on 1/21/2019 5:18:15 AM.

The metallogelation of tetradentate ligands **3** and **4** was also studied in various DMSO : H_2O ratios. Due to the solubility issues, more DMSO or DMF was needed than water in these solvent mixtures. Gelation was observed with 8 : 2, 7 : 3 (Fig. 3) and 6 : 4 DMSO : H_2O ratios when the gelation concentration is 0.4 wt% for ligands **3** and **4**. However, stable gels were obtained only when 7 : 3 DMSO : H_2O was used. To determine the optimum ligand-to-metal ratio to obtain stable gels, experiments using the L : M molar ratio of 2 : 1, 1 : 1, 1 : 2, 1 : 3 and 1 : 4 were carried out using $AgNO_3$ in 7 : 3 DMSO : H_2O. When ligand-to-metal ratio 2 : 1 was used no gelation was observed (Fig. S11b, ESI†). However, the addition of an excess of $AgNO_3$ resulted in short lived unstable gels. The optimum ligand-to-metal ratio to obtain a truly stable gel was found to be 1 : 1. This suggests that silver(I) ions are tetracoordinated. Therefore, all the further studies were carried out in 7 : 3 DMSO : H_2O and 1 : 1 ligand-to-metal ratio for **3** and **4**. Ligand **3** formed metallogels in all the tested silver salts (Table 1). Similar studies using ligand **4** revealed again metallogelation for all the tested salts. However, most of them were unstable except the ones containing PF_6^- and OAc^- anions. The above gelation studies thus indicate that ligands **1** and **3** display similar behaviour, whereas ligands **2** and **4** differ from **1** and **3** but show similar metallogelation abilities among each other. Our results are in good agreement with the literature, where the effect of the counteranion in metallogels has been well documented.[3a] The metallogels were found to gradually loose water and undergo precipitation upon heating. A similar observation has been reported for other coordination polymer metallogels in the literature.[16] The effect of temperature on the gels can also be monitored using variable temperature (VT) NMR spectroscopy.[36] It has been shown that under VT ^{1}H NMR experiments, the broad signals turn sharper and undergo a clear splitting upon gel melting in the case of thermoreversible gels.[36e] On the other hand, the lack of gel–sol transition will show no significant change upon heating close to the boiling point of the solvent.

The effect of temperature on the **[1_2·AgPF$_6$]** gel (DMSO-d_6:D_2O) was studied by performing VT ^{1}H NMR experiments from 30–80 °C (Fig. S12, ESI†) with 10 °C increment step. Ligand **1** alone in DMSO-d_6 displayed characteristic sharp peaks. However, when ligand **1** alone was measured in 3 : 7 DMSO : H_2O, all signals showed upfield (shielded) shift with slight broadening. Addition of Ag(I) in the form of $AgPF_6$, resulted in gelation and signal broadening (Fig. S12c–i, ESI†). Moreover, all of the signals arising from ligands showed downfield (deshielded) shift upon adding silver salt. Increasing the temperature showed increasingly sharp peaks with a clear splitting of all the resonance signals at 80 °C. After heating, the NMR tube contained a brownish coloured solution with a precipitate at the bottom of the NMR tube (Fig. S12, ESI†). The above results suggest that the gel undergoes partial melting. Furthermore, above 60 °C, there is a slight upfield shift of the signals and the position of the resonance signals is close to that of the gel at room temperature. This indicates that the signals observed in the gel state might arise from mobile components. Similarly, for ligand **3**, an upfield shift was observed when 7 : 3 DMSO-d_6–D_2O was used compared to that of DMSO-d_6 alone. When silver salt was added to the ligand solution no prominent signals were observed indicating immediate gelation. Upon heating above 50 °C broad signals were visible and even at 90 °C they remained broad (Fig. S13 and S14, ESI†). The sample did not show any visual melting at 90 °C suggesting that the gel is not undergoing gel–sol transition under the experimental conditions.

To gain further insights, 1D (^{1}H and ^{13}C) and 2D (^{1}H–^{1}H) correlation NMR spectroscopy (COSY), ^{1}H–^{13}C heteronuclear multiple bond correlation (HMBC) and ^{1}H–^{15}N COSY NMR spectroscopic measurements were performed for ligands **1–4** and their Ag-complexes in solution. Upon metal complexation, a significant change in the chemical shifts for the protons was observed (see the ESI,† for ^{1}H NMR spectral comparison). To probe the effect of metal coordination, 2D ^{1}H–^{15}N correlation spectroscopy for free ligands and their Ag-complexes was performed in DMSO-d_6.[30] Fig. 4a shows ^{1}H–^{15}N 2D-COSY of the free ligand **1** and Fig. 4b of its 2 : 1 metal complex **[1_2·AgNO$_3$]**. Upon complexation, an obvious change in the chemical shift values of nitrogen atoms was observed. The nitrogen atoms (N1 and N3) of ligand **1** showed an upfield shift of 6.84 and 10.62 ppm respectively, which is a clear indication of the coordination of both the nitrogen atoms from the ligand. The NMR spectroscopic results and the optimum ligand-to-metal ratio needed for stable metallogels suggesting possible tetracoordination of Ag(I) ions. This observation is further supported by single

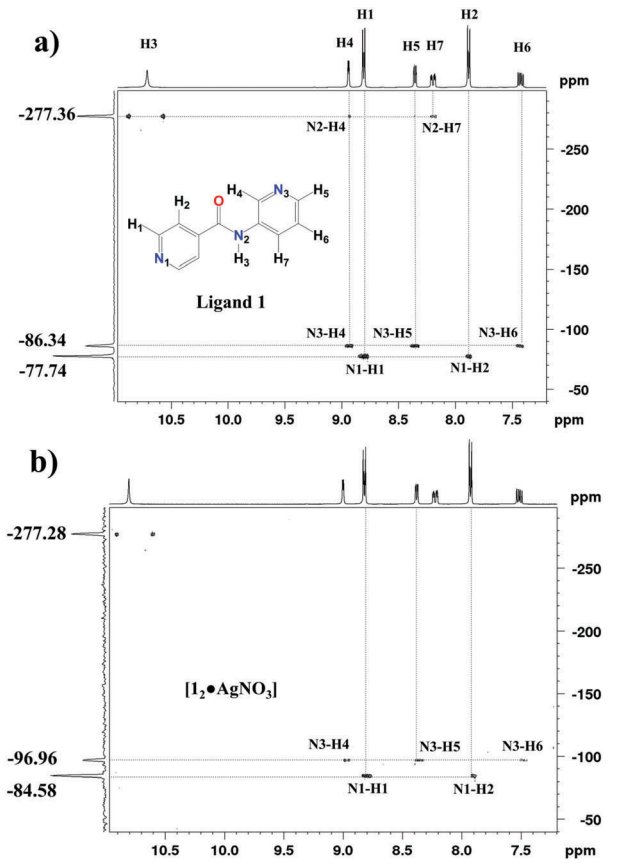

Fig. 4 ^{1}H–^{15}N 2D correlated spectrum of ligand **1** and **[1_2·AgNO$_3$]** in DMSO-d_6 at 30 °C.

Published on 11 December 2018. Downloaded by Gothenburg University Library on 1/21/2019 5:18:15 AM.

crystal X-ray structures of $\mathbf{1_2{\cdot}AgX}$ showing coordination polymerization directed by tetracoordinated Ag(I) ions. The 2D ^{1}H–^{15}N correlation spectra of ligand **3** and its complex $\mathbf{[3{\cdot}AgNO_3]}$ (Fig. S7, ESI†) were measured at 70 °C due to their solubility issues. Even at this high temperature, a significant upfield shift from the nitrogen atoms of bipyridine (N1) and pyridine (N3) moieties was observed and the shift is 4.35 and 4.57 ppm respectively.

The position of the counter anion in the Ag-complex was predicted based on ^{1}H NMR spectral results. The NH signals of **1** (Fig. S1, ESI†) and **3** (Fig. S4, ESI†) showed a downfield shift of 0.07 and 0.04 ppm respectively, in their Ag-complexes. The above observation was further clarified by performing ^{19}F NMR spectra of pure $AgFP_6$ and its gels with ligand **1** and **3** (see the ESI,† Fig. S15). Significant upfield chemical shifts were observed for gels prepared from **1** (2.66 and 2.65 ppm) and **3** (9.56 and 10.40 ppm) respectively. This suggests the presence of intermolecular H-bonding between the hydrogen atoms from the amide group and counter anions, which can be seen in the solid-state structure of silver CPs with the ligand **1**. Based on the molar ratio of bipyridine ligands (**3** or **4**) to **AgX** (1 : 1) and the NMR spectral analysis, the complex was assigned as CP where the silver cation is tetrahedrally coordinated by one chelating bipyridine unit and two bridging pyridine rings from adjacent ligands (Fig. 5 and Fig. S16, ESI†).

In order to understand detailed packing and interactions involved in coordination polymerization, we investigated the X-ray crystal structure of CPs. The crystallization of **1** with silver(I) in 7 : 3 or 8 : 2 (v/v) of DMSO : H_2O water (*i.e.* non-gelling conditions) leads to the formation of single crystals or precipitates. The reaction of **1** with AgX (X = ClO_4^-, OTf^- and PF_6^-) at 2 : 1 molar amounts gave two-dimensional coordination polymers (2D-CPs) where the silver was tetra coordinated by four individual ligand molecules.[35] The $\mathbf{[1_2{\cdot}AgClO_4]}$ (Fig. 6a), $\mathbf{[1_2{\cdot}AgOTf]}$ (Fig. 6b), and $\mathbf{[1_2{\cdot}AgPF_6]}$[37] (Fig. S20, ESI†) were crystallized in monoclinic space group $P2_1/n$. These 2D layers interact further with each other through counter anions *via* classical N–H···O and several weak C═C–H_{Py}···O, and C═C–H_{Py}···F hydrogen bonds (Table S3, ESI†) to immobilize the solvent molecules. A one-dimensional ladder type coordination polymer was obtained from the reaction of **1** with AgOAc. The $\mathbf{[1{\cdot}AgOAc]}$ (Fig. 6c) was crystallized in triclinic space group $P\bar{1}$. Similarly, each silver atom is tetra coordinated by two ligand molecules and two bridging acetate molecules to form an infinite ladder type architecture. These ladders are further self-assembled to generate a 2D layered structure *via* N–H···O hydrogen bonding involving amide N and acetate O atoms of the adjacent chains (N···O = 2.760(2) Å).

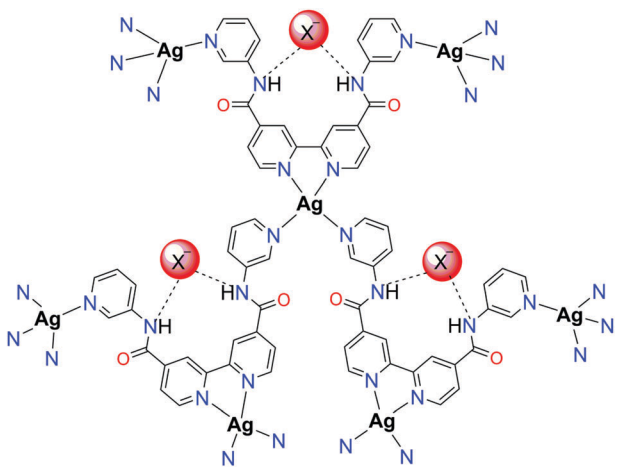

Fig. 5 The proposed structure of the coordination polymer $\mathbf{[3{\cdot}AgX]_n}$ (X = NO_3^-, ClO_4^-, OTf^-, PF_6^- and BF_4^-) in a solution and gel.

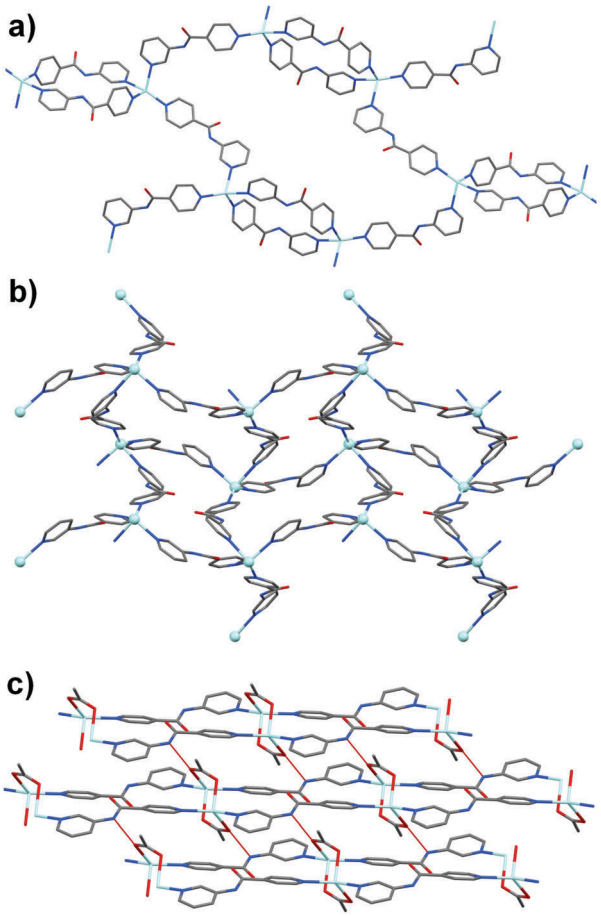

Fig. 6 Crystal packing of 2D-CPs of $\mathbf{[1_2{\cdot}AgClO_4]}$ (a), $\mathbf{[1_2{\cdot}AgOTf]}$ (b) and 1D-CP of **[1·AgOAc]** (c). Hydrogen atoms and counter anions (ClO_4^- and $CF_3SO_3^-$) are omitted for clarity.

The packing patterns in the single crystals and gel phase may be different as the gelation conditions are different from that of crystallization. To test this hypothesis, the powder X-ray diffraction (PXRD) was carried out for the xerogel derived from $\mathbf{[1_2{\cdot}AgClO_4]}$. The PXRD patterns of the xerogel with the simulated XRD patterns of the single crystal of $\mathbf{[1_2{\cdot}AgClO_4]}$ were found to be similar (Fig. S21, ESI†). The results suggest that in the xerogel there exists similar packing arrangement for metal complexes.

Morphology and *in situ* nanoparticle formation

The morphological features of the gels were investigated using electron microscopy for all 24 metallogels studied in this work.

This journal is © The Royal Society of Chemistry 2019

Published on 11 December 2018. Downloaded by Gothenburg University Library on 1/21/2019 5:18:15 AM.

The transmission electron microscopy (TEM) suggested that the metallogels derived from **[1_2·AgX]** and **[2_2·AgX]** form either film-like or rod-like networks depending on the counter anions (Fig. 7). Whereas, the metallogels derived from **[3·AgX]** and **[4·AgX]** showed highly entangled fibrillar networks except with $AgBF_4$. The most interesting finding from this work is the *in situ* formation of ultrasmall nanoparticles ($d < 3$ nm). Fig. 7 shows representative TEM micrographs from **[1_2·AgX]** and **[3·AgX]** with various silver salts. While most of the gels showed the formation of fibres with uniformly distributed ultrasmall silver nanoparticles ($d < 3$ nm), the perchlorate and acetate furnished film-like structures with uniformly distributed nanoparticles. Larger particles (5–20 nm) were also observed in the case of **[1_2·AgOAc]** gels. Whereas, the gels derived from **[3·AgX]** and **[4·AgX]** (see the ESI†) showed both ultrasmall and larger (5–20 nm) nanoparticles. This is also evident from the surface plasmon resonance (SPR) spectra of the gels (Fig. S23, ESI†). As in the case of gels derived from **[1_2·AgX]** and **[2_2·AgX]**, they show the formation of ultrasmall AgNPs uniformly distributed along the fibres and film-like materials. However, in addition to ultrasmall nanoparticles, the gels derived from **[3·$AgPF_6$]**, **[3·$AgClO_4$]** and **[3·$AgBF_4$]** also showed the formation of larger polydispersed nanoparticles. It should be noted that the pyridine, bipyridine and 1,10-phenanthroline based ligands have been explored previously for the synthesis of AgNPs using additional reducing agents with a considerable degree of uncontrolled aggregation of as formed nanoparticles. Furthermore, a vast majority of the previous reports represent larger nanoparticles with $d > 5$ nm. Remarkably, the present work shows the formation of ultrasmall silver nanoparticles, that are well dispersed within the gel matrix and fibres. HR-TEM of small nanoparticles (Fig. 7d and p) revealed the lack of lattice fringes. This behaviour is well documented in the literature for nanoparticles having a size below 2 nm due to the non FCC packing of atoms.[38] Furthermore, ultrasmall nanoclusters are also electron beam sensitive. However, for larger nanoparticles, HR-TEM displayed lattice fringes (Fig. 7h and l) that are typical for plasmonic silver nanoparticles.

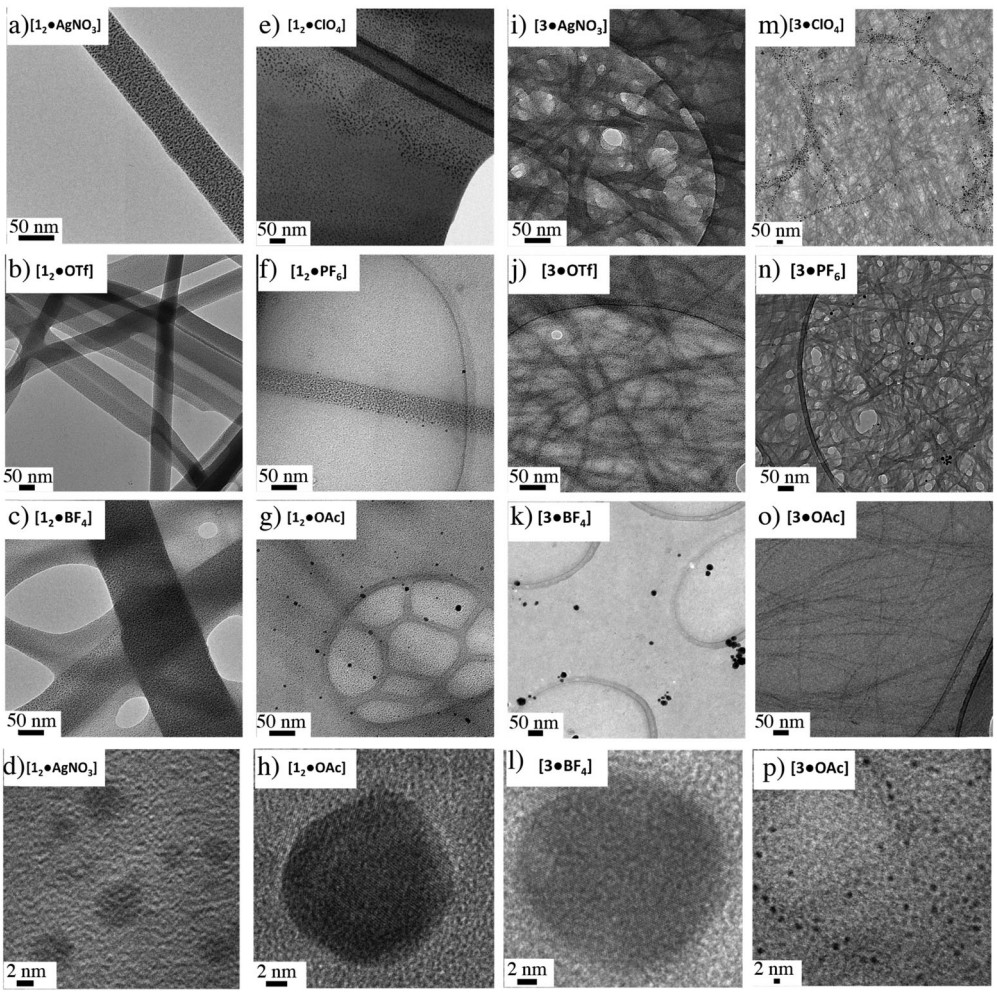

Fig. 7 TEM micrographs of metallogels. Representative TEM micrographs of metallogels derived from six different salts with ligand **1** (a–h), and ligand **3** (i–p), showing the gel fibres and films with *in situ* formed silver nanoparticle. Representative HR-TEM of individual nanoparticles in metallogels from ligand **1** (d and h), and ligand **3** (l and p) showing the lattice fringes in larger nanoparticles.

Published on 11 December 2018. Downloaded by Gothenburg University Library on 1/21/2019 5:18:15 AM.

Rheology of metallogels

The mechanical properties of metallogels are affected by the ligand chemical structures and metal ions as well as the counter anions. TEM imaging suggests that the morphological features and nanoparticle formation, as well as their arrangement within the gel matrix, depends on the ligand as well as the counter anions (Fig. 7). To gain insights into the mechanical properties of the gels, rheological measurements of the metallogels were performed. The gels for rheological experiments were prepared by adding aqueous solution of silver salt to a solution of the ligand in DMSO to achieve the final DMSO : H_2O ratio of 3 : 7 for ligands **1** and **2** and 7 : 3 for ligands **3** and **4**. Accordingly, the following gels (0.8 wt%) were used for rheological measurements in duplicate, **[1_2·AgNO$_3$]**, **[1_2·AgPF$_6$]**, **[1_2·AgBF$_4$]**, **[1·AgOAc]**, **[2_2·AgOTf]**, **[3·AgNO$_3$]**, **[3·AgClO$_4$]**, **[3·AgOTf]**, **[3·AgPF$_6$]**, **[3·AgBF$_4$]**, **[3·AgOAc]**, and **[4·AgOAc]**. All other gels were unstable under the experimental conditions or upon transferring the gels for the rheological measurements (see Experimental section). The stability of the gels was monitored using time sweep experiments, performed within the linear viscoelastic regime (0.1% strain) with 6.29 rad s^{-1} under the controlled temperature for 30 min. Time sweep experiments are useful to determine the sol–gel transition by monitoring the elastic (G') and loss modulus (G''). However, in our experiments, the pre-stabilized gels were used. For all the gels G' was found to be higher than G'' indicating the viscoelastic nature of the materials and the gels remained stable under the experimental conditions (Fig. 8). Similarly, the frequency sweep experiments showed that G' of the gels is higher than G'', confirming that the materials under study are viscoelastic in nature. For a given ligand the strength of the gels depends strongly on the counter anion. For metallogels derived from ligand 1, **[1_2·AgX]** the elastic modulus G' was found to follow the order $BF_4 > PF_6 > NO_3 > OAc$ with values of 69, 60, 49 and 11 Pa, respectively (see the ESI,† Fig. S22a and b). Furthermore, for a given silver salt the gel strength strongly depends on the ligand chemical structure. When AgOAc was used as the silver salt the metallogels derived from ligand **4** were found to be strongest and those with ligand **1** was found to be relatively weak. The G' values are 406, 43 and 11 Pa, for **[4·AgOAc]**, **[3·AgOAc]** and **[1_2·AgOAc]**, respectively (see the ESI,† Fig. S22e and f). The strain sweep experiments also reveal the viscoelastic properties of the gels under investigation. The rheological properties of viscoelastic materials are independent of strain and show linear viscoelastic behaviour below a certain level known as the critical strain, and the materials remain highly structured. Above the critical strain the G' shows a sharp decline and a cross-over between G' and G'' ($G'' > G'$) suggests gel–sol transition. Comparison of a strain sweep experiment between **[1_2·AgNO$_3$]** (Fig. 8c) and **[3·AgNO$_3$]** (Fig. 8f) metallogels, shows that above 10% strain the gels undergo transition into sol. However, the modulus of **[1_2·AgNO$_3$]** shows a continuous decline even below 10% strain, suggesting that the gels are not highly structured. On the other hand, **[3·AgNO$_3$]** gels display linear behaviour below 10% strain, and a sharp decline above the critical strain. Therefore, there exists a significant difference in the gel network structures between the two metallogels. This observation is also evident from TEM images, where **[3·AgX]** forms highly entangled fibrillar networks, whereas **[1_2·AgX]** shows rod-like or crystallites (Fig. 7). Therefore, metallogels derived from ligand **3** display better rheological properties compared to the metallogels derived from ligand **1**.

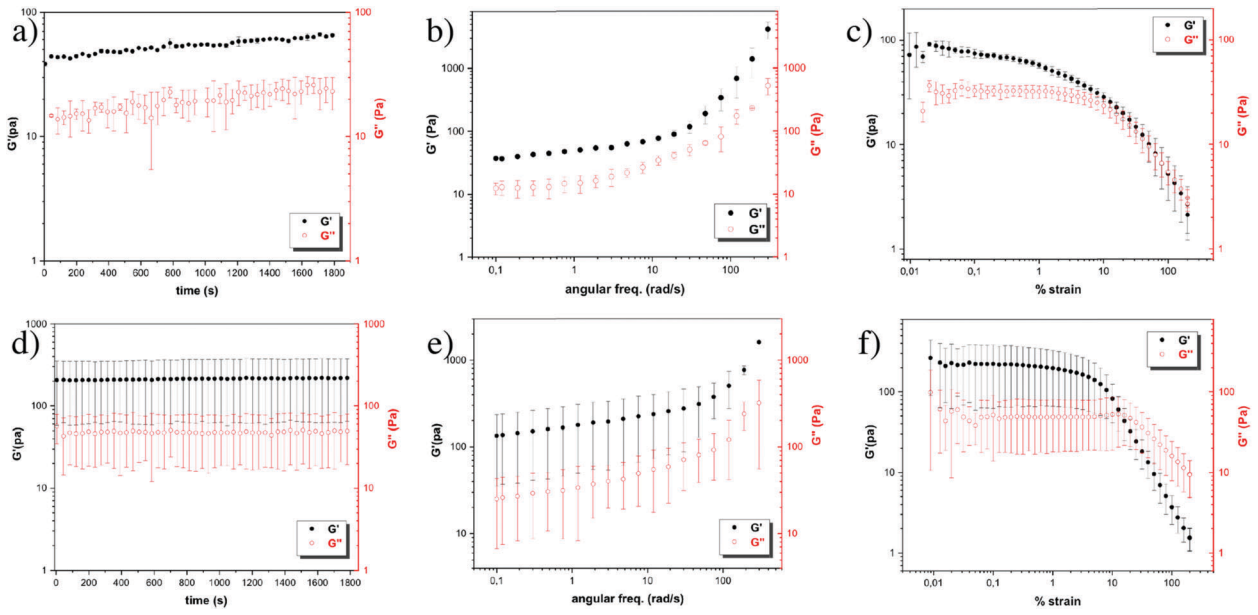

Fig. 8 Selected rheological properties of metallogels. (a–c) Time sweep, frequency sweep and strain sweep experiments of **[1_2·AgNO$_3$]**. (d–f) Time sweep, frequency sweep and strain sweep experiments of **[3·AgNO$_3$]**. Filled black circles represent the storage modulus (G') and empty red circles represent the loss modulus (G''). Time sweep experiments were performed at a frequency of 6.283 rad s^{-1} and 0.1% strain; frequency sweeps were collected at a strain value of 0.1% and strain sweeps were collected at a frequency of 6.283 rad s^{-1}.

 This journal is © The Royal Society of Chemistry 2019

Published on 11 December 2018. Downloaded by Gothenburg University Library on 1/21/2019 5:18:15 AM.

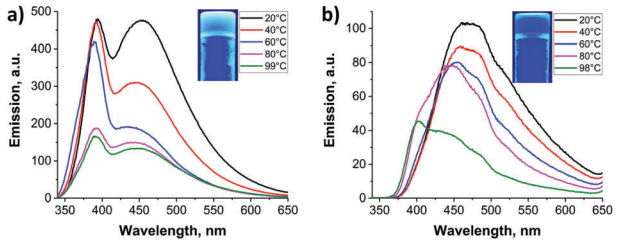

Fig. 9 Variable temperature emission spectra of the coordination polymers **[1_2·AgPF$_6$]** (a) and **[3·AgPF$_6$]** (b) under excitation at 300 nm.

Photoluminescence

Another interesting finding in our study is the self-assembly induced photoluminescence displayed by all the metallogels studied in this work. Accordingly, the photoluminescence properties of metallogels prepared from ligands **1–4** with **AgX** in a mixture of DMSO and water were investigated. We used the $AgPF_6$ since it resulted in stable gels upon complexation with all the ligands (Table 1). All the gels displayed emission in the visible range upon photoexcitation at 300 nm (see Fig. S24a, ESI†).‡ Emission measurements at different temperatures revealed that the luminescence intensity decreases upon heating of the gels (Fig. 9 and Fig. S24b, c, ESI†), indicating a key role of gelation in their luminescence properties.

No significant influence of the anion on luminescence was observed within the PF_6 and NO_3 series (Fig. S19e and f, ESI†). Comparison of the emission spectra of the gel prepared from ligand **2** alone and metallogel **[2_2·AgPF$_6$]** (Fig. S24d, ESI†) reveals essentially the same emission wavelength, even though the emission intensity of the metallogel is several orders of magnitude lower, probably facilitated by silver(I) singlet–triplet transitions.[39] This allows for the preliminary assignment of luminescence of the metallogels understudy to intraligand π*–π or π*–n transitions.

This suggestion is also supported by a similarity between the emission spectra of solids **1** and **2** (Fig. S25, ESI†) and their silver metallogels, which has also been observed for other **1**-based coordination polymers.[40] At the same time, **3** and **4** based metallogels display red-shifted emission compared to pure solid ligands. This observation can be attributed to the chelation of silver atoms by bipyridyl moieties, resulting in the shift of luminescence emission.

Conclusions

Metallogels are a continuously evolving area in metallosupramolecular chemistry. Silver(I) coordinated metallogels offer many additional properties such as spontaneous *in situ* silver nanoparticle formation, and optical and mechanical properties. They are also model systems to understand the structural details, the interactions involved in the self-assembly and gelation. This work demonstrates that structurally simple pyridyl and bipyridyl amides lead to an unprecedented self-assembly induced gelation, photoluminescence and rapid access to ultrasmall nanoparticles. Noble metal ultrasmall nanoparticles have been gaining considerable attention in recent years because of their unique size and shape dependent optical properties and possibilities to construct hierarchical colloidal superstructures. The structural details obtained by X-ray crystallography studies are useful towards the rational design of new gelators with novel functionalities.

‡ Low emission intensity and slight dependence of emission on orientation of the gel sample were observed due to low transparency of the gels. All emission spectra of the gels displayed emission bands with maxima at 362 and 393 nm, which is attributed to the solvent admixture and its intensity depends on the sample transparency.

Experimental section

Metal complexes

[1_2·AgNO$_3$]: ^{1}H NMR (300 MHz, DMSO-d_6) δ 10.78 (s, 1H), 8.99 (d, 1H), 8.82 (dd, 2H), 8.37 (dd, 1H), 8.22 (dq, 1H), 7.92 (dd, 2H), 7.50 (q, 1H). ^{13}C NMR (75 MHz, DMSO-d_6) δ 164.32, 150.70, 145.61, 142.42, 141.64, 135.65, 128.41, 124.17, 121.88. ^{1}H–^{15}N COSY NMR (DMSO-d_6 at 30 °C) δ −84.58 (carbonyl pyridine N^C), −96.96 (amino pyridine N^N) and −277.29 (amide nitrogen N^A).

[2_2·AgNO$_3$]: ^{1}H NMR (300 MHz, DMSO-d_6) δ 10.95 (s, 1H), 8.83 (dd, 2H), 8.54 (dd, 2H), 7.89 (dd, 2H), 7.86 (dd, 2H).

[3·AgNO$_3$]: ^{1}H NMR (300 MHz, DMSO-d_6) δ 10.94 (s, 1H), 9.00 (d, 2H), 8.96 (d, 1H), 8.39 (dd, 1H), 8.24 (dq, 1H), 8.05 (dd, 1H), 7.48 (q, 1H). ^{13}C NMR (75 MHz, DMSO-d_6 at 80 °C) δ 163.94, 154.95, 149.89, 144.92, 142.79, 142.21, 134.94, 127.62, 123.12, 121.95, 118.56.

^{1}H NMR (500 MHz, DMSO-d_6 at 70 °C) δ 10.80 (s, 1H), 8.99 (d, 2H), 8.95 (d, 1H), 8.38 (dd, 1H), 8.22 (dq, 1H), 8.03 (dd, 1H), 7.46 (q, 1H). ^{1}H–^{15}N COSY NMR (DMSO-d_6 at 70 °C) δ −64.35 (Bipy N^B), −67.23 (Py N^P) and −253.16 (Amide N^A).

[4·AgNO$_3$]: No solubility was found.

Gelation procedure

In a typical gelation experiment, an appropriate amount of solid ligand (**1–4**) was placed in a test tube (l = 45 mm, d = 15 mm) and dissolved in DMSO upon heating, whereupon an aqueous solution of the corresponding silver salt (**AgX**) was added to reach a final volume of 1.0 mL. The mixture was then cooled down to room temperature, which furnished a translucent/transparent gel or precipitate depending on the ligand and silver salt.

X-ray crystallography

The single crystals of **4** and silver CPs from **1** were immersed in cryo-oil, mounted in a MiTeGen loop and measured at 120 K. The X-ray diffraction data were collected on an Agilent Technologies Supernova diffractometer using Mo Kα radiation. The *CrysAlisPro*[41] program packages were used for cell refinements and data reductions. Structures were solved by the intrinsic phasing *SHELXT*[42a] program. Analytical or multi-scan absorption correction was applied to all data and structural refinements were carried out using *SHELXL*[42b] and Olex2 graphical user interface software.[43] The crystallographic details are given in the ESI.†

Published on 11 December 2018. Downloaded by Gothenburg University Library on 1/21/2019 5:18:15 AM.

Transmission electron microscopy (TEM)

The transmission electron microscopy (TEM) images were collected using an FEI Tecnai G2 operated at 120 kV and JEM 3200FSC field emission microscope (JEOL) operated at 300 kV in bright field mode with an Omega-type Zero-loss energy filter. The images were acquired with GATAN DIGITAL MICROGRAPH software. The TEM samples were prepared by placing 3.0 μL of the gel onto a 300 mesh copper grid with a holey carbon support film. The TEM grids were plasma cleaned prior to use. The samples were dried under ambient conditions prior to imaging.

Rheological measurements

A TA AR2000 stress-controlled rheometer equipped with a 20 mm steel plate and a Peltier heated plate was used for rheological characterization. The gels were prepared by adding a known volume of aqueous silver salt to a known volume of ligand in DMSO in an 8 mL vial with a screw cap to achieve 3 : 7 or 7 : 3 DMSO : H_2O for ligands **1** and **2** and ligands **3** and **4**, respectively. The solution of ligands in DMSO was prepared by heating over an oil bath until a clear solution was obtained. The temperature of the ligand solution in DMSO was maintained at 40–50 °C. An appropriate amount of an aqueous solution of salt was added to the warm ligand solution to obtain homogeneous gels. Addition of salt solution at room temperature resulted in inhomogeneous gels or precipitates. The gels were then allowed to stand at room temperature (~22 °C). The reheating of the gels was challenging due to precipitation, direct loss of water and rapid colour change due to uncontrolled silver nanoparticle formation. Therefore, *in situ* gelation on a rheometer remained a challenge. Therefore, only those gels that are stable for scooping were studied for their rheological properties. Accordingly the gels were then transferred to the rheometer by scooping. It is important to note that, scooping might disturb the gel structure. The measuring setup was covered with a sealing lid in order to prevent evaporation during the measurements. Measurements were performed using 0.1% strain and the oscillation frequency of 6.289 rad s^{-1} (1 Hz) at 20 °C unless otherwise noted. All the measurements were carried out in duplicate and the rheological data were analyzed using the TA Universal Analysis software.

UV-Vis and photoluminescence measurements

ACS reagent grade DMSO (≥99.9%) was used for all optical measurements. UV-Vis and photoluminescence spectra were recorded using Perking Elmer Lambda 650 and Varian Cary Eclipse Fluorescence Spectrophotometers respectively. Gel samples were prepared directly in 1 cm quartz cuvettes with care to produce as transparent gels as possible. Samples of the solid ligands were measured as thin layers of ground powder pressed between quartz plates.

Conflicts of interest

There are no conflicts to declare.

Acknowledgements

RT and MH kindly acknowledge the financial support from the Academy of Finland (M. H. Proj. no. 295581). Academy of Finland, Centre of Excellence in Molecular Engineering of Biosynthetic Hybrid Materials (HYBER, 2014–2019) and the Aalto University Nanomicroscopy Center (Aalto-NMC) are kindly acknowledged for the use of their facilities. COST Action 1302 "Smart Inorganic Polymers" is also acknowledged as a valuable source of inspiration.

Notes and references

1 S. Leininger, B. Olenyuk and P. J. Stang, *Chem. Rev.*, 2000, **100**, 853–908.
2 S. Kitagawa, R. Kitaura and S. Noro, *Angew. Chem., Int. Ed.*, 2004, **43**, 2334–2375.
3 (*a*) M.-O. M. Piepenbrock, G. O. Lloyd, N. Clarke and J. W. Steed, *Chem. Rev.*, 2010, **110**, 1960–2004; (*b*) Y. He, Z. Bian, C. Kang and L. Gao, *Chem. Commun.*, 2010, **46**, 5695–5697; Y. He, Z. Bian, C. Kang and L. Gao, *Chem. Commun.*, 2011, **47**, 1589–1591; (*c*) L.-J. Chen, Y.-Y. Ren, N.-W. Wu, B. Sun, J.-Q. Ma, L. Zhang, H. Tan, M. Liu, X. Li and H.-B. Yang, *J. Am. Chem. Soc.*, 2015, **137**, 11725–11735.
4 S. Bhowmik, B. N. Ghosh and K. Rissanen, *Org. Biomol. Chem.*, 2014, **12**, 8836–8839.
5 (*a*) K. Chen, L. Tang, Y. Xia and Y. Wang, *Langmuir*, 2008, **24**, 13838–13841; (*b*) P. Sutar and T. K. Maji, *Chem. Commun.*, 2016, **52**, 8055–8074.
6 (*a*) J. B. Beck and S. J. Rowan, *J. Am. Chem. Soc.*, 2003, **125**, 13922–13923; (*b*) X. Yan, D. Xu, X. Chi, J. Chen, S. Dong, X. Ding, Y. Yu and F. Huang, *Adv. Mater.*, 2012, **24**, 362–369.
7 J. Zhang and C.-Y. Su, *Coord. Chem. Rev.*, 2013, **257**, 1373–1408.
8 A. Y.-Y. Tam, K. M.-C. Wong and V. W.-W. Yam, *J. Am. Chem. Soc.*, 2009, **131**, 6253–6260.
9 (*a*) X. Yu, L. Chen, M. Zhang and T. Yi, *Chem. Soc. Rev.*, 2014, **43**, 5346–5371; (*b*) A. V. Zhukhovitskiy, M. Zhong, E. G. Keeler, V. K. Michaelis, J. E. P. Sun, M. J. A. Hore, D. J. Pochan, R. G. Griffin, A. P. Willard and J. A. Johnson, *Nat. Chem.*, 2016, **8**, 33–41.
10 (*a*) M. Burnworth, L. Tang, J. R. Kumpfer, A. J. Duncan, F. L. Beyer, G. L. Fiore, S. J. Rowan and C. Weder, *Nature*, 2011, **472**, 334–337; (*b*) G. E. Giammanco, C. T. Sosnofsky and A. D. Ostrowski, *ACS Appl. Mater. Interfaces*, 2015, **7**, 3068–3076; (*c*) M. Mauro, S. Bellemin-Laponnaz and C. Cebrian, *Chem. – Eur. J.*, 2017, **23**, 17626–17636.
11 (*a*) S.-I. Kawano, N. Fujita and S. Shinkai, *J. Am. Chem. Soc.*, 2004, **126**, 8592–8593; (*b*) S. Sarkar, S. Dutta, S. Chakrabarti, P. Bairi and T. Pal, *ACS Appl. Mater. Interfaces*, 2014, **6**, 6308–6316; (*c*) Y. Zhang, B. Zhang, Y. Kuang, Y. Gao, J. Shi, X. X. Zhang and B. Xu, *J. Am. Chem. Soc.*, 2013, **135**, 5008–5011; (*d*) K. Mitsumoto, J. M. Cameron, R.-J. Wei, H. Nishikawa, T. Shiga, M. Nihei, G. N. Newton and H. Oshio, *Chem. – Eur. J.*, 2017, **23**, 1502–1506.
12 C. Wang, D. Zhang and D. Zhu, *J. Am. Chem. Soc.*, 2005, **127**, 16372–16373.

 This journal is © The Royal Society of Chemistry 2019

Published on 11 December 2018. Downloaded by Gothenburg University Library on 1/21/2019 5:18:15 AM.

13 T. Kishida, N. Fujita, K. Sada and S. Shinkai, *Langmuir*, 2005, **21**, 9432–9439.
14 Y. Cho, J. H. Lee, J. Jaworski, S. Park, S. S. Lee and J. H. Jung, *New J. Chem.*, 2012, **36**, 32–35.
15 (*a*) J. H. Lee, S. Kang, J. Y. Lee and J. H. Jung, *Soft Matter*, 2012, **8**, 6557–6563; (*b*) L. Yan, L. Shen, M. Lv, W. Yu, J. Chen, S. Wang, X. Fu and Z. Ye, *Chem. Commun.*, 2015, **51**, 17627–17629; (*c*) S. Ganta and D. K. Chand, *Dalton Trans.*, 2015, **44**, 15181–15188; (*d*) S.-L. Yim, H.-F. Chow, M.-C. Chan, C.-M. Che and K.-H. Low, *Chem. – Eur. J.*, 2013, **19**, 2478–2486.
16 P. Casuso, P. Carrasco, I. Loinaz, G. Cabanero, H. J. Grande and I. Odriozola, *Soft Matter*, 2011, **7**, 3627–3633.
17 (*a*) J. J. Marrero-Tellado and D. D. Díaz, *CrystEngComm*, 2015, **17**, 7978–7985; (*b*) A. Husain, R. Parveen and P. Dastidar, *Cryst. Growth Des.*, 2015, **15**, 5075–5085.
18 (*a*) K. K. Kartha, V. K. Praveen, S. S. Babu, S. Cherumukkil and A. Ajayaghosh, *Chem. – Asian J.*, 2015, **10**, 2250–2256; (*b*) R. Tatikonda, S. Bhowmik, K. Rissanen, M. Haukka and M. Cametti, *Dalton Trans.*, 2016, **45**, 12756–12762.
19 (*a*) N. N. Adarsh, P. Sahoo and P. Dastidar, *Cryst. Growth Des.*, 2010, **10**, 4976–4986; (*b*) H. Bunzen, Nonappa, E. Kalenius, S. Hietala and E. Kolehmainen, *Chem. – Eur. J.*, 2013, **19**, 12978–12981.
20 R. G. Weiss, *J. Am. Chem. Soc.*, 2014, **136**, 7519–7530.
21 A. Y.-Y. Tam and V. W.-W. Yam, *Chem. Soc. Rev.*, 2013, **42**, 1540–1567.
22 (*a*) S. Bhowmik, B. N. Ghosh, V. Marjomaki and K. Rissanen, *J. Am. Chem. Soc.*, 2014, **136**, 5543–5546; (*b*) Q. Lin, T.-T. Lu, X. Zhu, B. Sun, Q.-P. Yang, T.-B. Wei and Y.-M. Zhang, *Chem. Commun.*, 2015, **51**, 1635–1638.
23 (*a*) P. Chen, Q. Li, S. Grindy and N. Holten-Andersen, *J. Am. Chem. Soc.*, 2015, **137**, 11590–11593; (*b*) P. Sutar, V. M. Suresh and T. K. Maji, *Chem. Commun.*, 2015, **51**, 9876–9879; (*c*) K. Hong, Y. K. Kwon, J. Ryu, J. Y. Lee, S. H. Kim and K. H. Lee, *Sci. Rep.*, 2016, **6**, 29805, DOI: 10.1038/srep29805; (*d*) P. Sutar and T. K. Maji, *Inorg. Chem.*, 2017, **56**, 9417–9425.
24 M. J. Bryant, J. M. Skelton, L. E. Hatcher, C. Stubbs, E. Madrid, A. R. Pallipurath, L. H. Thomas, C. H. Woodall, J. Christensen, S. Fuertes, T. P. Robinson, C. M. Beavers, S. J. Teat, M. R. Warren, F. Pradaux-Cassiano, A. Walsh, F. Marken, D. R. Carbery, S. C. Parker, N. B. McKeown, R. Malpass-Evans, M. Carta and P. R. Raithby, *Nat. Commun.*, 2017, **8**, 1800, DOI: 10.1038/s41467-017-01941-2.
25 L. Arnedo-Sanchez, Nonappa, S. Bhowmik, S. Hietala, R. Puttreddy, M. Lahtinen, L. DeCola and K. Rissanen, *Dalton Trans.*, 2017, **46**, 7309–7316.
26 (*a*) B. Xing, M.-F. Choi and B. Xu, *Chem. – Eur. J.*, 2002, **8**, 5028–5032; (*b*) Y.-R. Liu, L. He, J. Zhang, X. Wang and C.-Y. Su, *Chem. Mater.*, 2009, **21**, 557–563.
27 L. Qin, P. Wang, Y. Guo, C. Chen and M. Liu, *Adv. Sci.*, 2015, **2**, 1500134, DOI: 10.1002/advs.201500134.
28 (*a*) M.-O. M. Piepenbrock, N. Clarke and J. W. Steed, *Soft Matter*, 2011, **7**, 2412–2418; (*b*) H. Svobodová, Nonappa, M. Lahtinen, Z. Wimmer and E. Kolehmainen, *Soft Matter*, 2012, **8**, 7840–7847; (*c*) M. Cametti and Z. Džolić, *Chem. Commun.*, 2014, **50**, 8273–8286; (*d*) I. Pastoriza-Santos and L. M. Liz-Marzán, *Langmuir*, 1999, **15**, 948–951.
29 P. Rajamalli, P. Malakar, S. Atta and E. Prasad, *Chem. Commun.*, 2014, **50**, 11023–11025.
30 (*a*) K. Nath, A. Husain and P. Dastidar, *Cryst. Growth Des.*, 2015, **15**, 4635–4645; (*b*) M. Paul, K. Sarkar and P. Dastidar, *Chem. – Eur. J.*, 2015, **21**, 255–268.
31 R. Tatikonda, K. Bertula, Nonappa, S. Hietala, K. Rissanen and M. Haukka, *Dalton Trans.*, 2017, **46**, 2793–2802.
32 (*a*) M. Oh and C. A. Mirkin, *Nature*, 2005, **438**, 651–654; (*b*) A. I. d'Aquino, Z. S. Kean and C. A. Mirkin, *Chem. Mater.*, 2017, **29**, 10284–10288; (*c*) X. Sun, S. Dong and E. Wang, *J. Am. Chem. Soc.*, 2005, **127**, 13102–13103; (*d*) X. Sun, S. Dong and E. Wang, *Chem. Soc. Rev.*, 2009, **38**, 1218–1227.
33 C. Zimmer, M. Hafner, M. Zender, D. Ammann and R. W. Hartmann, *Bioorg. Med. Chem. Lett.*, 2011, **21**, 186–190.
34 D. K. Kumar, D. A. Jose, P. Dastidar and A. Das, *Langmuir*, 2004, **20**, 10413–10418.
35 CCDC 1823427–1823433 contains the supplementary crystallographic data for this paper†.
36 (*a*) Nonappa and E. Kolehmainen, *Soft Matter*, 2016, **12**, 6015–6026; (*b*) Nonappa, M. Lahtinen, B. Behera, E. Kolehmainen and U. Maitra, *Soft Matter*, 2010, **6**, 1748–1757; (*c*) V. Noponen, Nonappa, M. Lahtinen, A. Valkonen, H. Salo, E. Kolehmainen and E. Sievänen, *Soft Matter*, 2010, **6**, 3789–3796; (*d*) Nonappa and E. Kolehmainen, *Gels*, 2016, **2**, 9; (*e*) Nonappa, D. Saman and E. Kolehmainen, *Magn. Reson. Chem.*, 2015, **53**, 256–260.
37 K. Uemura, *Inorg. Chem. Commun.*, 2008, **11**, 741–744.
38 R. Jin, C. Zeng, M. Zhou and Y. Chen, *Chem. Rev.*, 2016, **116**, 10346–10413.
39 R. Tatikonda, E. Bulatov, E. Kalenius and M. Haukka, *Cryst. Growth Des.*, 2017, **17**, 5918–5926.
40 (*a*) J. A. Wilson and R. L. LaDuca, *Inorg. Chim. Acta*, 2013, **403**, 136–141; (*b*) T. A. Beard, J. A. Wilson and R. L. LaDuca, *Inorg. Chim. Acta*, 2017, **466**, 30–38.
41 Rigaku Oxford Diffraction, CrysAlisPro., Yarnton, Oxfordshire, England, 2013.
42 (*a*) G. M. Sheldrick, *Acta Crystallogr., Sect. A: Found. Adv.*, 2015, **71**, 3–8; (*b*) G. M. Sheldrick, *Acta Crystallogr., Sect. C: Struct. Chem.*, 2015, **71**, 3–8.
43 O. V. Dolomanov, L. J. Bourhis, R. J. Gildea, A. J. K. Howard and H. Puschmann, *J. Appl. Crystallogr.*, 2009, **42**, 339–341.